CrossMark

Growth behavior of preferentially scalloped intermetallic compounds at extremely thin peripheral Sn/Cu interface

Shengyan Shang[1] · Anil Kunwar[2] · Yanfeng Wang[1] · Lin Qu[1] · Haitao Ma[1] · Yunpeng Wang[1]

Abstract
The growth behaviour of Cu_6Sn_5 intermetallic compound (IMC) at the solder height controlled post-spread Sn/Cu interface is investigated for different initial solder ball volumes, reflow temperatures and cooling rates. Because of the limited solder thickness at the periphery, the IMC retains a preferential scalloped morphology, even after cooling. For solder balls of initial diameters of 500, 1000 and 1700 μm, with the maximum solder height at the peripheral regime not exceeding 150 μm, reflowed at 250 °C and undergoing air cooling, it has been revealed that IMC characterized with larger layer thickness and grain diameter, correspond to the sample of smaller ball size. The increase in reflow temperature for a solder of initial size of 500 μm, is characterized by the increase in IMC thickness, developments of few but quite large faceted planes over the original scalloped morphology and non-uniformity in the grain diameter. In contrary the to air cooling (cooling rate ≥ 4.0 K/s), the IMCs obtained at the thin film zone, for furnace cooling (cooling rate = 0.037 K/s), are very larger, both in grain size and layer thickness. Moreover, the scalloped Cu_6Sn_5 surface in furnace cooled specimens, bear many but tiny facets. Finite element analysis is utilized to numerically estimate the diffusion of Cu into the geometrical volumes of solder. Ostwald ripening and film height are the important parameters defining the growth behavior of the compound in miniaturized solder joints.

1 Introduction

In electronic packaging sector and solar photo voltaic (PV) manufacturing industries, there is an ongoing research trend regarding the reliability of Pb-free solder alloys. The environmental and human health related benefits of lead-free Sn-based solders are the motivating factors to encourage the researchers and technologist to study about these alloys. Some of the key reliability issues for solder joints, such as Sn electrodeposits and whiskers [1, 2], voids and bubbles [3], thermomigration [4] and electromigration [5], introduced by the reaction between Sn based alloys solder and Cu substrate, which are related about the formation of intermetallic compounds (IMCs) [6, 7]. The topic of IMC is considered in the scope of this present study, and particularly, Cu_6Sn_5

intermetallic compound was generalized as IMC owing to its rapid occurrence during reflow soldering of solder joints. Though the formation of Cu_6Sn_5 IMC is necessary to guarantee the establishment of solder joint, too much thick IMCs are not desirable because of the brittle property of Cu_6Sn_5 compound.

The development of three-dimensional integrated circuit (3D IC) packaging technology [8–11], has caused the solder interconnect to downsize to balls of diameter < 50 μm. Moreover, the Cu_6Sn_5 IMC growth related to this size effect poses a serious reliability concern [12–17]. Any study providing relationship between solder volume and intermetallics compound, can be added in contributing for the reliability enhancement of solder joints. In most of the existed research works about effect of solder size on Cu_6Sn_5 IMC growth behavior; the characteristic dimensions of the solders considered are larger than 150 μm, owing to the difficulty of preparing the smaller sized solder volumes. A few researchers [15, 18] have succeeded in forming Cu/μm-solder/Cu joints, with the size of μm-solder ≤ 50 μm. However, it is a known fact that too smaller samples are difficult not only from the aspect of fabrication but also from the viewpoint of characterization.

✉ Haitao Ma
htma@dlut.edu.cn

✉ Yunpeng Wang
yunpengw@dlut.edu.cn

1 School of Materials Science and Engineering, Dalian University of Technology, Dalian 116024, China

2 School of Mechanical Engineering, Dalian University of Technology, Dalian 116024, China

When solder balls of sizes 500–2000 μm melted and spread over Cu substrate, during the interfacial energy driven viscous flow of Sn based material over Cu radially outward, the decreasing solder thickness also varies radially: thickest at the center and thinnest at the periphery [19]. In this context, the thin solder film at the peripheral strip, with thickness <150 μm can be considered as a practical case of possessing an interface with a smaller solder height. As this method is practically far easier than making extremely small specimens, it can be utilized widely in investigating interfacial kinetics in miniaturized solder joints. Moreover, it has already been reported in Ref. [19, 20] that the morphologies of intermetallics compound at the peripheral and central interfaces, are different. However, these works are limited to solder of a given initial volume and thus, do not report the size effect.

For this study, in order to avoid the influence of Cu and Ag elements on the IMC growth, the pure Sn solder was chosen. The reflow of pure Sn solder balls of initial diameters 500, 1000 and 1700 μm at 250 °C over Cu substrates, subsequently allow them to spread over them and finally subject them to undergo air cooling. The mechanism of the size effect on the interfacial reaction has been studied by many researchers, the exact mechanism of how height and the width of solder bulk influence the shape of Cu_6Sn_5 crystal during soldering process is not clear. To understand the size effect for miniaturized Sn films, we investigate the IMC evolution of the peripheral regime of the post-spread solder. Thus, an experimental study regarding the IMC growth behavior at the peripheral-only liquid solder/Cu interface using solder balls of several initial volumes, can provide very useful data about miniaturized solder joints. In addition to the initial solder ball sizes (and subsequent peripheral film dimensions), a further experiment is performed on a given sized solder-substrate system to assess the roles of reflow temperatures and cooling rates, on the Cu_6Sn_5 IMC growth behavior of a. A very slow cooling rate is applied by conducting furnace cooling after reflow experiment. Considering the utmost significance of non-destructive experiments [21], especially for cooling experiment, in situ visualizations results are provided by performing synchrotron radiation imaging experiments on air cooling and furnace cooling procedures, for a Sn/Cu interface, with solder height around or < 100 μm.

2 Experimental methods and numerical formulation

2.1 Materials and experiments

Pure Sn solder ball (Dalian Golden Saddle Welding Limited Company, China; purity: 99.99%, melting point:231.89 °C),

polycrystalline Cu substrate (Qingyuan Metal Materials Limited Company, China; purity: 99.99%, melting point: 1083.4 °C), rosin flux (AMTECH:NC-559-ASM) were utilized for the preparation of solder joints. The Cu material that is used as a substrate in this experiment, had a dimension of 15 mm × 5 mm × 100 μm. It was cleaned in 5% HCl solution (vol%) with ultrasonic vibration to remove the surface oxide film,then rinsed with deionized (DI) water and, finally dried in acetone for soldering.

After adding rosin flux to the substrate, the solder ball was placed onto Cu substrate. After that, put the solder/Cu system inside a reflow oven (Forced Convection, FT02) for single reflow maintained under the pressure of 1 atm. Initially spherical Sn solder balls of three initial diameters (500, 1000 and 1700 μm) were used for research on the size-effects to the growth behavior of Cu_6Sn_5 at the peripheral Sn/Cu interface of the post spread solders. The solders joints, thus named as D500, D1000 and D1700, in accordance to the magnitudes of initial diameters, were reflowed in the furnace for 120 s and then subjected to cooling. It is to be noted that the geometry of the solders spread on the substrate will be non-spherical as shown in Fig. 1, with the peripheral solder film relatively thinner. For the study of the influence of soldering temperature on Cu_6Sn_5 IMC growth behavior at the peripheral domain of the solder-substrate interface, the Sn/Cu specimens were reflowed at 250 °C, 275 °C and 300 °C and then subjected to air cooling. The air cooling (AC) experiment was carried out by immediately removing out the insulated frame or walls of the furnace once the heating power is turned off, and the reference time was considered at the point when the insulated frame or walls of the furnace was moved. For the investigation about the effect of cooling speed on the growth of Cu_6Sn_5 compounds, additional samples of D500 solder reflowed at 250 °C for 120 s and subjected to furnace cooling (FC). In order to start furnace cooling experiment, the insulated walls and windows of furnace were maintained in the oven even after the stoppage of heating power, and the reference time, t = 0, was considered at the point when the heater power was turned off in the furnace. The temperature within the furnace was measured by thermocouple (TC). Furthermore,
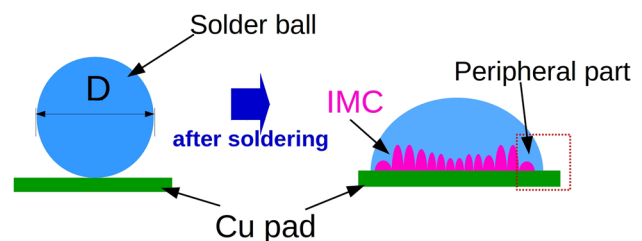

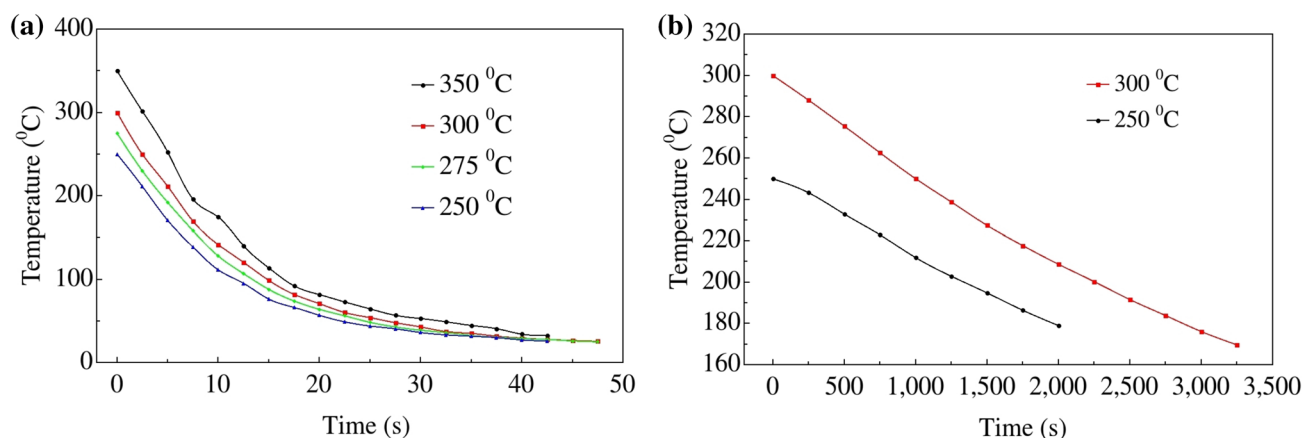**Fig. 1** The schematic diagrams for Sn/Cu solder bumps before and after reflow

(a)

(b)

Fig. 2 Experimental data of temperature (T) variation with time (t) during **a** air cooling and **b** furnace cooling

Fig. 3 Schematic sketch for experimental setup of synchrotron radiation in situ observation of IMC growth during cooling processes
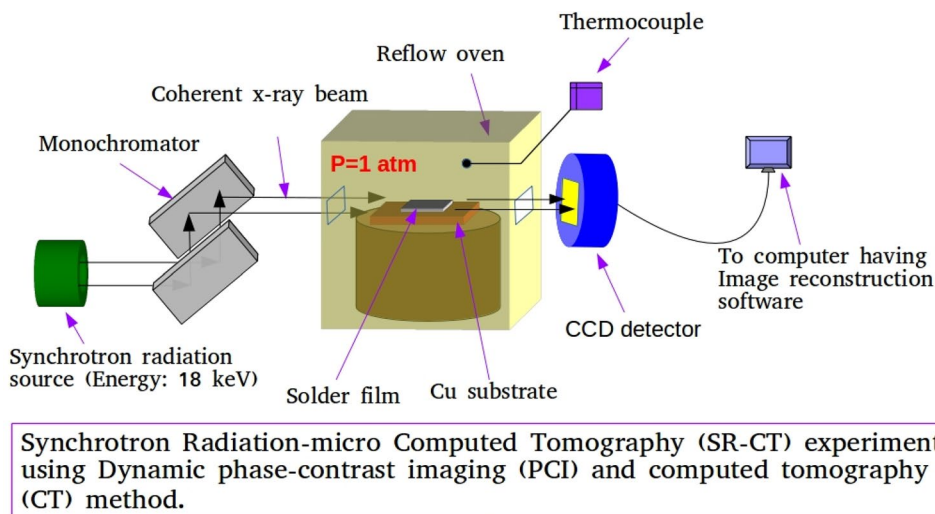

Synchrotron Radiation-micro Computed Tomography (SR-CT) experiment using Dynamic phase-contrast imaging (PCI) and computed tomography (CT) method.

Table 1 Cooling rate for experimental procedure

Cooling method	Reflow temperature (°C)	Cooling rate (K/s)
Air cooling	250	4.2
	275	4.4
	300	4.8
	350	6.1
Furnace cooling	250	0.037

the graphical plot of T–t curves for air cooling and furnace cooling are provided in Fig. 2. Similarly, the cooling rates for the experimental furnace and air cooling procedures are provided in Table 1.

In the aftermath of reflow and subsequent cooling, all samples were cleaned by ethanol with an ultrasonic bath. The bulk solder bump were removed by etching the samples with 10% HNO_3 solution (vol%). From this method, the top view interfacial Cu_6Sn_5 grains could be exposed on the Cu pad, which is convenient for the investigation of the top-view of IMC at the interface. At the same time, for the characterization of cross-section morphology, experimentally processed solder samples were polished, and slightly etched by 5 vol% HNO_3 + 2 vol% HCl + 93 vol% C_2H_5OH solution. Both the top-view and the cross-section microstructures were characterized with the equipment of scanning electron microscope (Zeiss Supra 55). The dimensions of samples were measured in accordance to Ref. [22].

For the in situ visualization of Cu_6Sn_5 growth under air cooling and furnace cooling condition, the experiment was carried out with synchrotron radiation X-ray imaging technique at the BL13W1 beam line of Shanghai Synchrotron Radiation Facility (SSRF) [23]. The experimental schematic sketch setup of synchrotron radiation is shown in Fig. 3. Monochromatic x-ray beam was placed over the interface of Sn/Cu joints during cooling procedure. Meanwhile, the pixels of 2D images of

the transmitted beam was captured by the CCD camera which was processed by computed tomography (CT) method. Before the cooling step started, the solders were reflowed at temperatures of 250 °C (furnace cooling) and 300 °C (air cooling). The energy of monochromatic X-ray beam of synchrotron radiation (SR) was 18 keV. The parameters of CCD camera, namely resolution ratio and exposure time, were respectively chosen as 0.325 μm/pix and 4 s. By utilizing the solid Cu substrate of thickness 100 μm, the penetration thickness of interface of the interface is constrained at this thickness value. Moreover, the height of the solder film during in situ visualization procedure is reduced to < 100 μm due to excessive spreading during reflow. And the results from dynamic phase contrast imaging (PCI) experiment can be correlated well with those of peripheral interfaces which was investigated via scanning electron microscopy (SEM). The whole experiment was carried out at an ambient pressure of 1 atm.

2.2 Numerical estimation of relative interfacial velocity for liquid Sn over Cu_6Sn_5 and Cu substrates

During reactive wetting, Cu_6Sn_5 intermetallic layer formed at the interface of liquid Sn and solid Cu will alter the spreading rate of the liquid [24]. In order to understand the role of IMC layer in changing the magnitude of spreading of Sn (reactive wetting), compared to pure Sn/Cu interface (dissolute spreading); separate cases of the representative volume elements (RVEs) consisting of Sn/IMC and Sn/Cu couples as shown in Fig. 4 are considered.

The evolution of non-conservative order parameters ϕ_i for a two phase (case I: liquid Sn and Cu_6Sn_5 phases; case II: liquid Sn and Cu phases) binary Cu–Sn system is described by the following Allen–Cahn equation [25, 26].

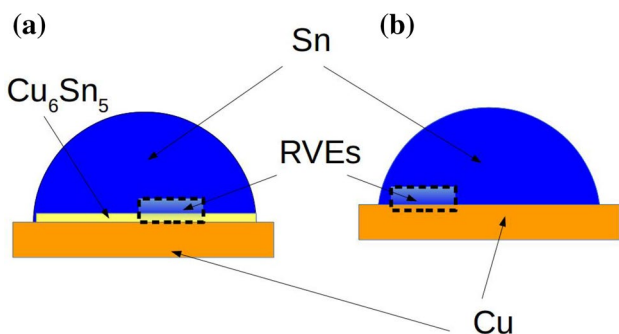$$\frac{\partial \phi_i}{\partial t} + v.\nabla\phi_i = -L_{\phi_i}\frac{\delta F}{\delta \phi_i} \qquad (1)$$

where, i = Sn, Cu_6Sn_5 for Fig. 4a and i = Sn, Cu for Fig. 4b. L_{ϕ_i} is kinetic mobility.

In the convection term of Eq. 1, v is the velocity in the computational domain. Navier–Stokes equation is utilized to describe the variation of velocity variable in the domain. The viscosity of liquid phase is taken in accordance to Ref. [27], whereas solid phases are chosen as regions of very high viscosities [25]. The free energy of the system is defined as the volume integral of free energy density [28]:

$$F = \int_\Omega f(c, \phi, \nabla\phi)d\Omega \qquad (2)$$

An expression $c = \Sigma_i h_i(\varphi) \times c_{sn}^i/V_m^i = \Sigma_i h_i(\varphi) \times [1 - c_{Cu}^i]/V_m^i$, consisting of interpolation function $h_i(\varphi)$, is used to relate the global molar concentration field (c) for a component (e.g. Sn or Cu) of Eq. 2, with molar fraction fields of conserved field variables (c_{sn}^i or c_{Cu}^i). The molar volumes V_m^i of Cu, Sn and IMC phases are taken as 7.12, 16.29 and 10.59 cm³/mol respectively. The free energy densities (f = G/V_m) [unit: J/m³] of Cu, Sn and IMC (η) phases at 250 °C are numerically evaluated in accordance to the values of Gibbs free energy (G) presented in curves of Fig. 5. In the phase field method based simulation, the interpolation
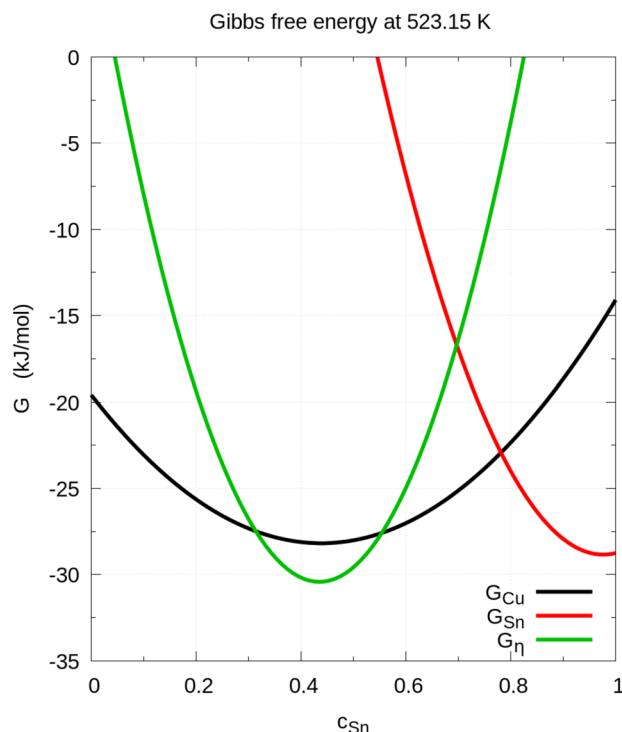

Fig. 4 The phases within representative elements corresponding to **a** Sn/Cu_6Sn_5 and **b** Sn/Cu pairs characterize a binary system

Fig. 5 The gibbs free energy curves for Cu, IMC (η) and Sn phases are shown in the image

function is utilized to switch the free energy density values within the several phases.

The surface energy occurring in the interfacial free energy density expression, for all the phases involved is taken as 0.5 J/m^2 [28]. In Eq. 2, c is the conserved variable representing the component c_i in i phases. The evolution of conserved variable is expressed by a Cahn–Hilliard equation coupled with convection term. The diffusion coefficients required for multiphase field simulation are obtained from [28, 29].

The Cahn–Hilliard, Allen–Cahn and Navier–Stokes equations are solved in MOOSE framework [30–34] for two phase ((I) Sn, η, (II) Sn, Cu) and two components (Sn, Cu) system. The law of equality of chemical potentials for several phases and mass conservation equation are solved in accordance to the requirement of Kim–Kim–Suzuki (KKS) model [35]. Let $v_{sn/\eta}$ and $v_{sn/cu}$ be the average velocities of liquid phase over IMC and Cu surface respectively as obtained from the computation of case I and case II choices of phases. Then the spread speed ratio (R), conceptualized as the factor to show the variation of non-reactive spreading with reactive wetting is defined as $\frac{v_{sn/cu}}{v_{sn/\eta}}$. The temporal evolution of R as computed through finite element analysis is shown in Fig. 6. For an initial liquid velocity in the range of 20–50 μm, it is noteworthy to mention that $v_{sn/cu}$ increases with time (in ms), whereas $v_{sn/\eta}$ of relatively smaller magnitude, first increase for a very short duration, and then decreases continually. The results of phase field calculation are in agreement to the inference presented in [25], wherein it is mentioned that the velocity of liquid for reactive wetting is smaller than that of non-reactive flows based Cox's hydrodynamic model [36].

The value of R can be used to divide the non-reactive spreading based velocity boundary conditions for use in numerical simulation of the following sections. Future work in the phase field model includes the design of more
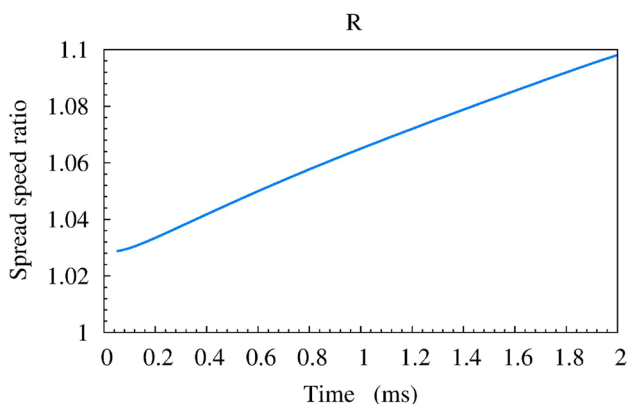
sophisticated reactive wetting system in a realistic geometry, with all the phases (Cu, Sn and IMC) being in simultaneous interaction with each other.

2.3 Finite element model for Cu diffusion in liquid solder

For the assessment of size effects of solder in Cu diffusion driven interfacial IMC growth during reflow at 250 °C, it is necessary to investigate the transient variation of Cu along the peripheral portion of the solder corresponding to the experimental samples representing the scallop only morphology (after air cooling). Thus, the domain of the numerical simulations are chosen as the peripheral portions of D500, D1000 and D1700. As the spread solders are assumed to be symmetrical, the representative volume element (RVE) for the finite element analysis is a peripheral solder volume at one quadrant. For a circular interface of a solder of total radius R (D/2; half of the diameter D), there is a critical radius (r_{crit}) from the center point, which separates the two regions with differentiated IMC morphologies. The IMCs inside r_{crit} bear prismatic grown over scalloped morphology, whereas those outside it are dominantly scalloped [19, 20]. In order to assess the zone with scallop only morphology, the thickness of circular strip at the peripheral zone, denoted as $\Delta L = L_{border} - L_{outermost} = L_{max} - 0.0 = L_{max} = R - r_{crit}$, is the basal dimension of the computational domain or RVE (It is considered that the thickness of peripheral strip is measured from outside). The subscript borders and outermost, respectively represent the morphology transition zone and triple line regime. Corresponding to the interfacial thickness, the heights of solder varies from $H_{outermost} = 0.0$ to $H_{border} = H_{max}$. The values of L_{max} and H_{max} for several samples are obtained from experimental method of demarcation respectively for width and height direction about IMC growth.

Three-dimensional geometries with meshes consisting of tetrahedral mesh elements are constructed in the preprocessing software—Salome 7.8.0 [37]. For the molten solder being in contact with the Copper(Cu) substrate at the bottom, Cu can diffuse into the solder medium. The transient evolution of Cu concentration within the liquid solder domain, denoted by C, can be expressed by the following advection-diffusion partial differential equation:

$$\frac{\partial C}{\partial t} = D\nabla^2 C - \vec{u}.\nabla C \qquad (3)$$

In Eq. 3, t is time and the unit of C is mol/cm^3. The diffusion coefficient (D) of Cu in molten Sn solder is 6.44×10^{-9} m^2/s at 250 °C [4, 38–41]. In the equation, $\vec{u}$ in the advection term, is the flow velocity of the liquid solder, and is obtained from incompressible Navier–Stokes equation. The flow of liquid within the solder domain is described by the incompressible Navier–Stokes equation as following:

Fig. 6 Calculated result of ratio R (t) for comparison of flow of liquid Sn between non-reactive system (Sn/Cu) and in a reactive system where Sn is assumed to be in contact with η phase

$$\nabla . \vec{u} = 0 \tag{4}$$

$$\rho \frac{\partial \vec{u}}{\partial t} + \rho (\vec{u}.\nabla)\vec{u} = \nabla.[-pI + \nu(\nabla\vec{u} + (\nabla\vec{u})^T)] + \vec{F}_{body} \tag{5}$$

where, p and ν are respectively the pressure and dynamic viscosity of the fluid Sn medium. The initial conditions for both the concentration of Cu in the solder, and velocity of the liquid, are considered as 0. In context of the plane boundary at the Sn/Cu interface; Dirichlet boundary condition (BC) = 3.00×10^{-3} mol/cc is chosen for the C variable [40]. Natural boundary conditions for C are defined in context of remaining boundaries of the computational domain. For imposing the velocity boundary conditions, the spreading of solder drops over Cu substrate at 250 °C, observed through synchrotron radiation imaging technique over intervals of 4 s was evaluated. The average velocity was determined for a total duration of 120 s . This velocity was then divided by R(t) determined in Sect. 2.2 to obtain the effective reactive spreading velocity. The effective velocity was applied as a BC to the liquid solder domain. With the initial condition and BCs defined for the system, Eq. 3 was solved along with Navier–Stokes equation using finite element method (FEM) in Elmer multiphysics software [3, 42]. Since the co-ordinate of the geometry was scaled by 1.0×10^{-3} in the finite element analysis (FEA), the time-step size was accordingly scaled to 0.001 s. Paraview 5.0.1 [43] is utilized for the post-processing and visualization tasks.

With the purpose of differentiating the Cu diffusion level in the peripheral and internal regimes which is driven by the geometrical spreading dynamics, an additional simulation work is carried out for total solder volume and inward section of sample D1700.

3 Results and discussion

3.1 Size effects on morphology of Cu_6Sn_5 IMC at peripheral interface

The magnitude of solder volume with a given Cu substrate has significant effect on the occurrence sizes of interfacial inner zone and peripheral strip. In the aftermath of cooling, the interface at inner zone may bear prismatic plus scalloped IMCs (in varying proportion), whereas the peripheral strip only consists of scalloped morphology. For the assessment of solder volume effects, samples air cooled from 250 °C are considered in this section. The Fig. 7 shows the top-view images of Cu_6Sn_5 at the interface of the Sn/Cu solder joints for samples (a) D500, (b) D1000 and (c) D1700. It reveals that the peripheral interface zone is characterized by only scalloped IMC morphology in context of all samples. With the inner zone interface composed of prismatic intermetallics compound growing over preexisting scalloped IMCs, the IMC morphology there can be described as mixed mode morphology. As the present study is more focused on the peripheral zone, it is tried to assess the peripheral solder dimensions on the growth behavior of intermetallics compound therein.

Figure 8 shows the cross-section view of the preferentially scalloped Cu_6Sn_5 at the peripheral Sn/Cu interface for reflow temperature of 250 °C followed by air cooling. From the Fig. 8, it revealed that even in the aftermath of air cooling, there is no occurrence of prismatic IMCs at the peripheral interface of Sn/Cu solder joint for all three size solder joint. In other words, the scalloped IMCs retained their morphology after them nucleate and grow via the mechanism of Ostwald ripening during isothermal reflow process at the peripheral interface.

However, the solder volume is shown to influence the radially inward length (L_{max}) of the peripheral interface from the triple line junction, and subsequently H_{max} as presented in Fig. 9. Both L_{max} and H_{max} are observed to increase with an increment in the solder volume. For D500, having spread
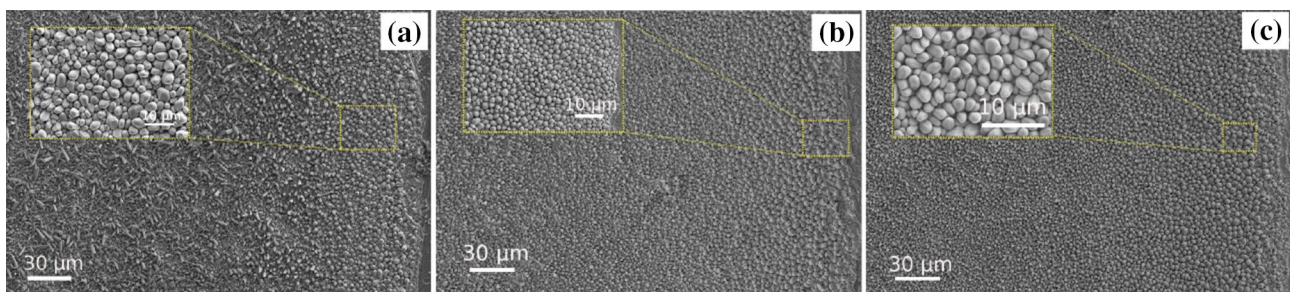

Fig. 7 The top-view images for Cu_6Sn_5 IMCs for samples **a** D500, **b** D1000 and **c** D1700 reflowed at 250 °C and subjected to air cooling. In all samples, the peripheral zone IMC is characterized by scalloped only IMC whereas the inner zone interface IMC bears mixed mode (differentially grown prismatic over scalloped shaped compounds) morphology
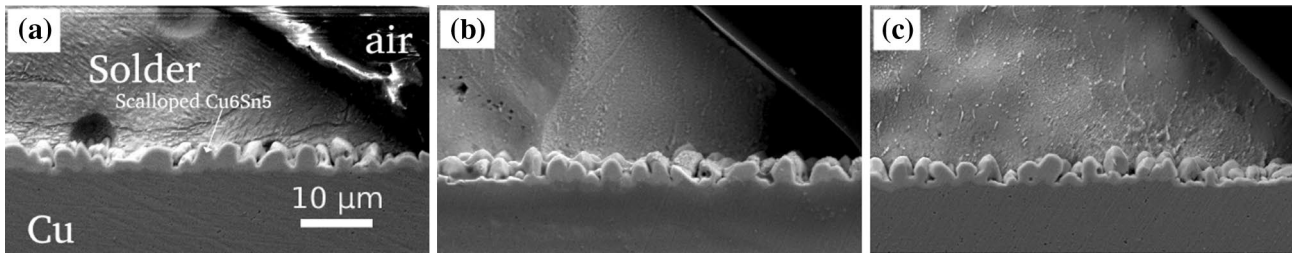
Fig. 8 The cross-section view of Cu_6Sn_5 intermetallic compounds at the peripheral Sn/Cu interface for samples **a** D500, **b** D1000 and **c** D1700 reflowed at 250 °C and being processed to undergo air cool-ing. The IMC is observed to preferentially retain scalloped morphol-ogy even after the completion of cooling
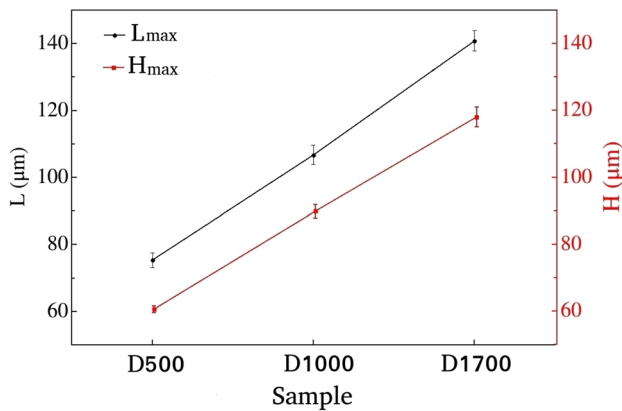

Fig. 9 The strip thickness values of the peripheral interface for sev-eral sized solder samples is depicted by the magnitude of L_{max}. Simi-larly, at the border regime between scalloped only and mixed mode IMC, the measured value of solder height is denoted as H_{max}

radius of base interface as 667 μm, the average values of L_{max} and H_{max} are measured to be 75 μm and 60 μm respec-tively. In context of D1700, whose post-spread basal radius is 1715 μm, the thickness of peripheral strip is 140 μm and the maximum solder height (H_{max}) for the occurrence of scalloped only morphology is 118 μm. The ratio $\frac{\Delta H}{\Delta L}$ is 0.80 at this peripheral zone for D500 and 0.84 for D1700. As the $\frac{\Delta H}{\Delta L}$ ratio is larger for D1700, it can be understood that, even after spreading, the the solder joint with larger diameter solder ball has a greater height at the border regime.

In context of sufficiently big Weber number (We), inertial force is found dominant for the spreading kinetics of molten

Sn solder on solid Cu substrate. Kinetically, for solder balls of initial drop radius ($R_{initial}$),the spreading rate (dr(t)/dt)for reaction limited spreading rate [44], can be written as as a function of time (t) as given below [45]:

$$\frac{dr(t)}{dt} = k\left(\frac{3V}{\pi}\right)^{\frac{1}{3}} F(\theta) \times exp^{-kt} \tag{6}$$

where, θ is instantaneous contact angle and V is the volume of solder ball.

From Eq. 6, it can be inferred that the spreading rate ($v = dr/dt$)) is larger for D1700 as compared to D500, since they have differing magnitudes of $R_{initial}$ [46]. This can explain the relative magnitudes of L_{max} and H_{max} for the different solder samples. Villanueva et al. [25] and Wang et al. [26], have performed phase field simulations to model reactive wetting, but still there is a dividing opinion about the actual start time of nucleation of IMCs at the interface during spreading procedure. Villanueva et al. [47] and Wang et al. [48], have assumed that dissolute wetting stage fol-lowed by intermetallic phase formation occur during total reactive wetting process; and thus ignore the competitive lateral spreading of intermetallics compound with respect to the contact line motion. Saiz et al. [49] mention that nucleation barrier for IMC formation causes the existence of time regime in which the lateral expansion of IMC lags the spread rate of solder liquid front, and in such situation the contact angle and spreading kinetics are respectively, governed by adsorption and ridge formation. The inferences from Eq. 6 and work of Saiz et al. [49], can be employed together to conceptualize the solder volume effect on the

Fig. 10 The transient distribu-tion of Cu concentration in liq-uid Sn solder during isothermal reflow for D1700 at 250 °C
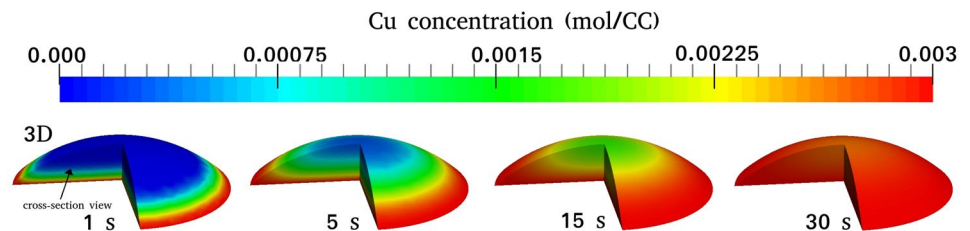
Fig. 11 Simulated results for illustration of difference between saturation levels of Cu concentration at the center part and the peripheral part of D1700 at t = 3 s during isothermal reflow at 250 °C

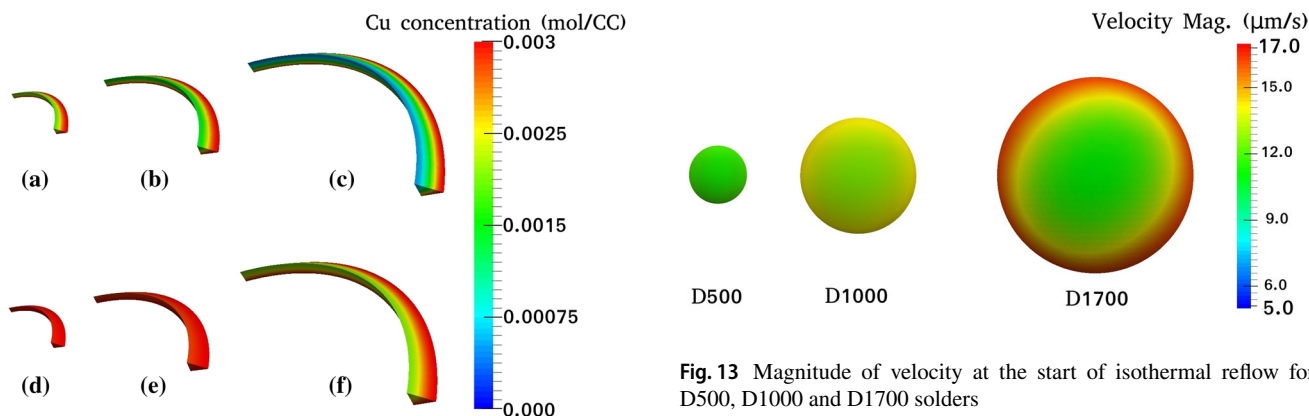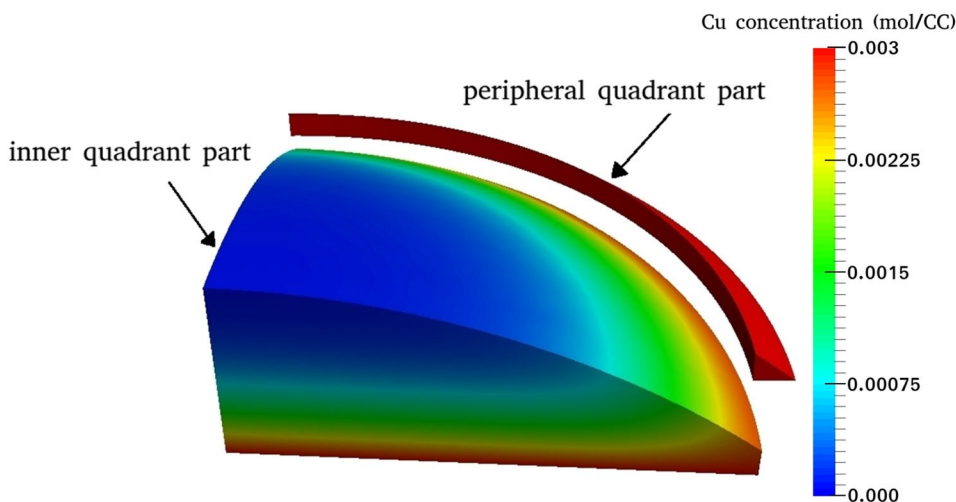**Fig. 12** The transient distribution of Cu concentration at peripheral part of liquid solder at 250 °C during isothermal reflow of D500, D1000 and D1700 respectively for **a**, **b** and **c** for 0.1 s and **d**, **e** and **f** for 0.3 s

Fig. 13 Magnitude of velocity at the start of isothermal reflow for D500, D1000 and D1700 solders

nucleation barrier induced IMC spread kinetics, which has a significant connotation to the present experimental design of this research.

3.2 Simulation results for Cu concentration and flow velocity during isothermal reflow stage

Figure 10 shows the transient Cu concentration of sectioned geometry of D1700 sample at the temperature = 250 °C. From these data, it is clearly observed that the Cu concentration get saturated at the peripheral part faster than the center part. At t = 1 s, the peripheral part that constitutes the solder over scalloped IMC portion is already saturated with Cu, whereas most of the central solder volume has lower Cu concentration. Till t = 30 s, when the central region starts gets saturated, the Cu concentration of peripheral solder film

already has been supersaturated. The difference in saturation level of Cu at t = 3 s, is shown in Fig. 11 for a one quarter of solder geometry, with central and peripheral volumes separated. The greater rate of Ostwald ripening kinetics due to supersaturation explains why the peripheral Cu_6Sn_5 IMCs are more preferentially scalloped.

As the peripheral regime already has been saturated with Cu within the first 1 s of soldering at 250 °C, the numerical results for Cu concentration at peripheral zones for D500, D1000 and D1700, are presented for simulation time < 1 s in Fig. 12. At t = 0.1 s, the upper solder volume of all three specimens are unsaturated with Cu with, that of D1700 being the least saturated. However, at t = 0.3 s, both D500 and D1000 are fully saturated with Cu solute, whereas the top portion of D1700 is still not saturated. Hence, smaller solder volume is more preferable for the formation of larger scalloped IMC grains owing to the flux driven ripening kinetics at the peripheral zone of the post-spread solders.

Figure 13 shows the simulation results of flow velocities' magnitudes for D500, D1000 and D1700 specimens, just after complete melting during the initial reflow
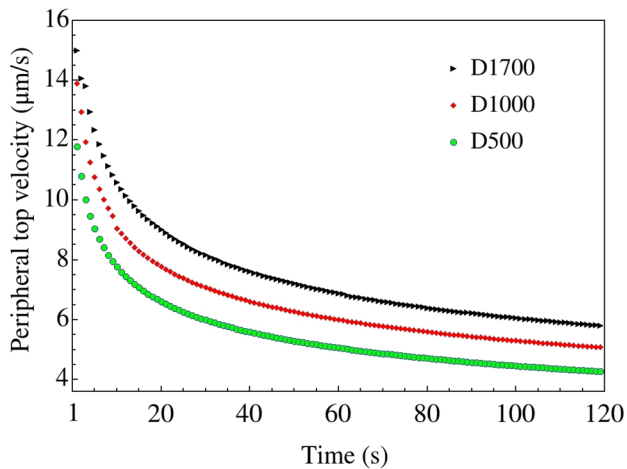
Fig. 14 Graphical plot of the variations of velocity at a top point in the solder periphery for different sized solders. The velocities decrease with the advent of time for all solder specimens

procedure. From the figure, it is evident that the largest solder D1700 is characterized by the greatest liquid velocity owing to its greater spreading rate. During initial reflow experiment at temperature of 250 °C, the maximum velocity for D1700 is 16.7 µm/s, whereas it is only 11.8 µm/s for smallest solder D500. The magnitudes of calculated velocities are in the similar order of the results obtained in Ref. [50]. Moreover, as revealed in the figure, the variation of velocity with solder height is more prominent with larger solder samples. D500 sample has a nearly uniform velocity regardless of the solder height from the spreading base. As shown in Fig. 14, the velocity at the top points of peripheral regime of solders decrease with the advent of time, which is caused by spreading rate of solder decreases with time. It is noteworthy to mention that the top point velocity is the larger for the bigger solder specimen. Thus, D500 has the smallest velocity and D1700 has the largest velocity, which is of utmost significance in solder joint reliability studies, due to the effect of liquid velocity in species distribution.

3.3 Effects of temperature and cooling rates on IMC growth behaviour

The magnitude of reflow temperature and cooling rates (CR) have a pronounced effect on the morphology and growth behavior of intermetallic compounds at the peripheral regime of the interface. For this investigation, the variation of temperature and cooling rates is conducted only for fixed solder volume and thus, D500 sample is chosen. Figure 15a–c
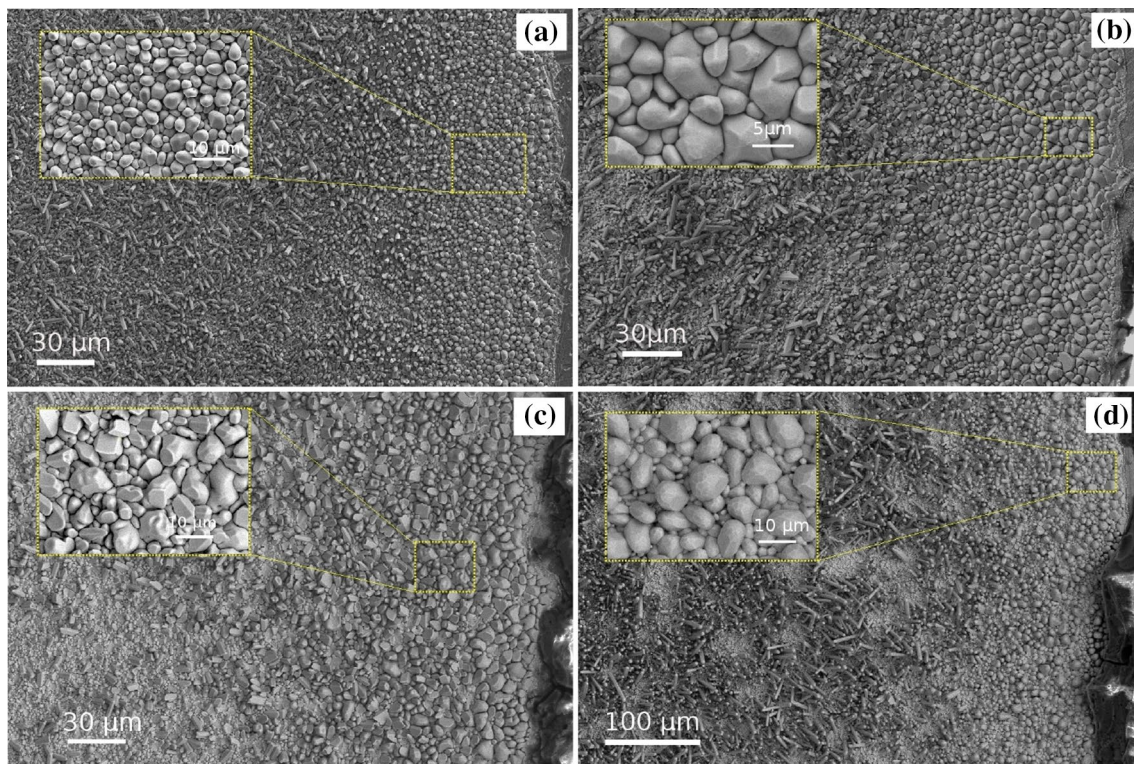

Fig. 15 Top-view image of IMC for sample D500 reflowed at temperature of **a** 250 °C, **b** 275 °C and **c** 300 °C, correspond to air cooling. The image **d** represents the morphology of IMC of D500 reflowed at 250 °C and followed by furnace cooling. As explained by the scale bars, the images for air cooling are magnified × 3.33 that of furnace cooling

shows the top-view of intermetallics compounds for solders reflowed at temperatures from 250, 275 and 300 °C and then air cooled. It is observed from the figure that, as the reflow temperature is increased or the air cooling rate (initiated by larger start temperature) is increased, the scalloped IMCs at the peripheral zone start bearing facets on them. One of the reason, is flux driven ripening kinetics is enhanced at larger reflow temperature, causing the IMCs to have bigger grain diameter and thus, faceted planes can appear in these large grains during cooling. In lower reflow temperature, the grain diameter of spherically capped IMCs is smaller and the facets occurring on tiny spheres are almost unnoticeable. The size of spherical scalloped caps during reflow also governs the diameter of prismatic IMCs that grow in the center region. In Fig. 15a, corresponding to 250 °C, the prismatic IMCs that grow over small scalloped grains are thin whiskers and are numerous. On the other hand, the prismatic compounds, that appear above the large scalloped grains of higher reflow temperature of 300 °C. As the Fig. 15c shows the IMC thickness are relatively thicker and are not so many in numbers. The cooling rate of 4 K/s has been reported in Ref. [51] as the maximum limit at which prismatic IMCs can form in the interface zone with sufficient solder volume. In context of reflow at 250 and 275 °C, the corresponding cooling rates, as shown in Table 1, are 4.2 and 4.4 K/s, and still prismatic IMCs which are thought to occur via the mechanism of screw dislocation [52, 53], can be found. However, as shown in Fig. 15c, consisting of sample air cooled from 300 °C, at a higher cooling rate of 4.8 K/s ($\approx$ 5 K/s), the screw dislocation mechanism based growth of IMCs is greatly suppressed and the central interface contains only a

few prismatic Cu_6Sn_5 compounds. Thus, from our present work, 5 K/s has been proposed as the maximum limit of cooling rate at which prismatic IMCs can sufficiently grow in the central region of the Sn/Cu interface. Fig. 15d reveals the top view morphologies of peripheral and central zones IMCs for D500 sample, with furnace cooling from a reflow temperature of 250 °C at a rate of 0.037 K/s. The grain diameters of scalloped IMCs at the peripheral zone for this sample are comparatively much more larger than all the air cooled samples, even than those reflowed at higher temperature. This is because that at extremely slower cooling rate for furnace cooling, Ostwald ripening kinetics can proceed well during the cooling procedure. For the contrast with the air cooled samples (from 275 and 300 °C) that contain fewer and larger facet planes within a scalloped grain at the periphery, the scalloped grains of furnace cooled specimen contain numerous and tiny facet planes within a scalloped grain. In context of air cooling (CR $\geq$ 4.0 K/s), Ostwald ripening kinetics immediately stops and precipitation kinetics driven action basically defines the morphology of post-cooled scalloped grains. On the other hand, in case of furnace cooling (CR $\approx$ 0.04 K/s), both Ostwald ripening [54] and precipitation driven grain growth [55], go hand in hand, during the extremely slow cooling procedure.

The results of the peripheral section, as shown by the top-view images, can also be conformed from corresponding cross-section view of Fig. 16a–d. For the air cooled samples of Fig. 16a–c, the increase of reflow temperature is enhanced by the formation of larger grains and more faceted scalloped IMCs. The IMC grain corresponding to 300 °C is relatively larger than the sample air cooled from 250 °C,

Fig. 16 The cross-section view of scalloped Cu_6Sn_5 at the peripheral Sn/Cu interface for air cooled D500 samples, initially reflowed at temperatures: **a** 250, **b** 275 and **c** 300 °C. Figure **d** shows IMC for same D500 sample that is furnace cooled from initial reflow temperature of 250 °C. As revealed by the scale bars, the images for air cooling are magnified three times that of furnace cooling
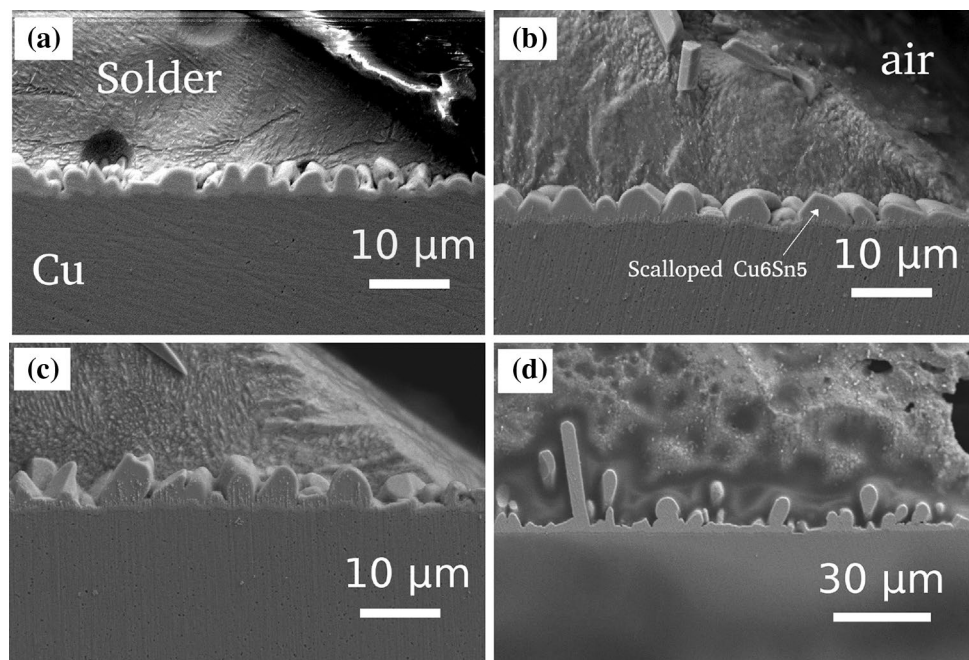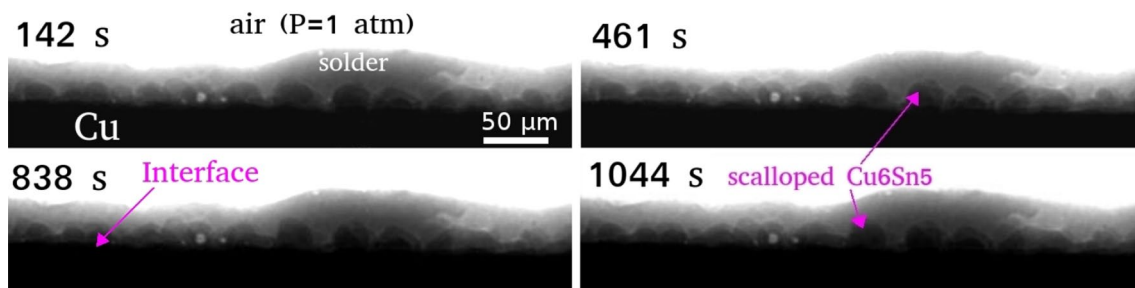
Fig. 17 The images for the Sn/Cu interface as obtained from SR-μmCT technique during air cooling in the aftermath of isothermal heating at 350 °C for reflow duration of 1.5 h
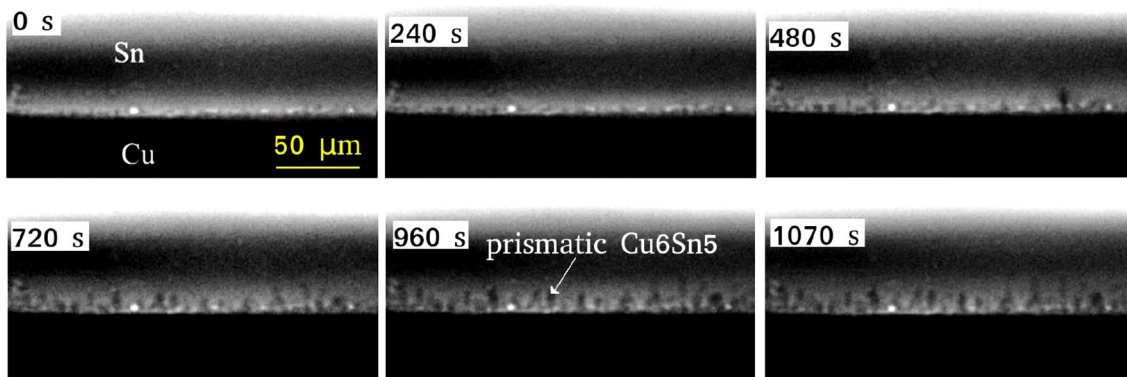

Fig. 18 Images obtained from synchrotron radiation X-ray imaging technique for liquid Sn/solid Cu interface subjected to furnace cooling after isothermal heating at 250 °C for reflow duration of 10 min. The start time t = 0 s refers to the point when the heater is turned off in the furnace

and the former contains notable facets. As the temperature increases, the Cu diffusion from substrate to the solder film of limited height, is faster, and solution is supersaturated at a great speed. With the liquid solution being saturated with a larger proportion of Cu more in context of higher isothermal reflow temperature, there will be enough Cu to precipitate at the interface to enable the screw dislocation driven growth of Cu_6Sn_5 and thus faceted planes appear at the surface of post-cooled Cu_6Sn_5 [19, 53]. It is noteworthy to mention that the scalloped IMCs of furnace cooled sample of Fig. 16d have much more larger grains than the air cooled samples. Moreover, these IMCs have rounded caps resulting from furnace cooling, which largely highlight the relative influence of Ostwald ripening during the cooling procedure.

Figures 17 and 18 represent the synchrotron radiation images of the interfacial Cu_6Sn_5 IMCs at the liquid Sn/solid Cu interface during air cooling and furnace cooling respectively. As the solder height is < 100 μm, the IMC growth can somehow mimic the practical condition of the inward part of the peripheral zone. During air cooling (CR ≈6.1 K/s), when the solder height is approximately 50 μm, the Cu_6Sn_5 IMCs bear scalloped morphology with larger grains. In context of furnace cooling for liquid solder height of 62

μm, at a cooling rate of 0.037 K/s, the IMCs show a clear prismatic morphology.

3.4 IMC grain size size and thickness

The measured values of intermetallics dimensions at peripheral zone for several solder samples and cooling conditions are provided in Fig. 19. For air cooling from an initial reflow temperature of 250 °C as depicted in Fig. 19a, the average IMC thickness are 2.68, 2.51 and 2.37 μm respectively for D500, D1000 and D1700 samples. Similarly, the mean IMC grain diameters for sample D500, D1000 and D1700, as given in Fig. 19c, are 3.97, 3.32 and 2.71 μm respectively. Thus, both the IMC grain diameter and thickness at the peripheral interface decrease with an increase in solder size or volume. With reference to the D500 sample, the percentage decrease in IMC thickness and grain diameters for D1700 samples are 11.57 % and 31.74 % respectively.

For D500 sample, corresponding to relow temperature of 250 °C, as illustrated by Fig. 19b, the mean IMC thickness for furnace cooling and air cooling are 5.22 and 2.68 μm respectively. The average grain size was shown in Fig. 19d, for FC and AC (both for reflow temperature = 250 °C) are 4.31 and 3.97 μm. Thus, after an isothermal
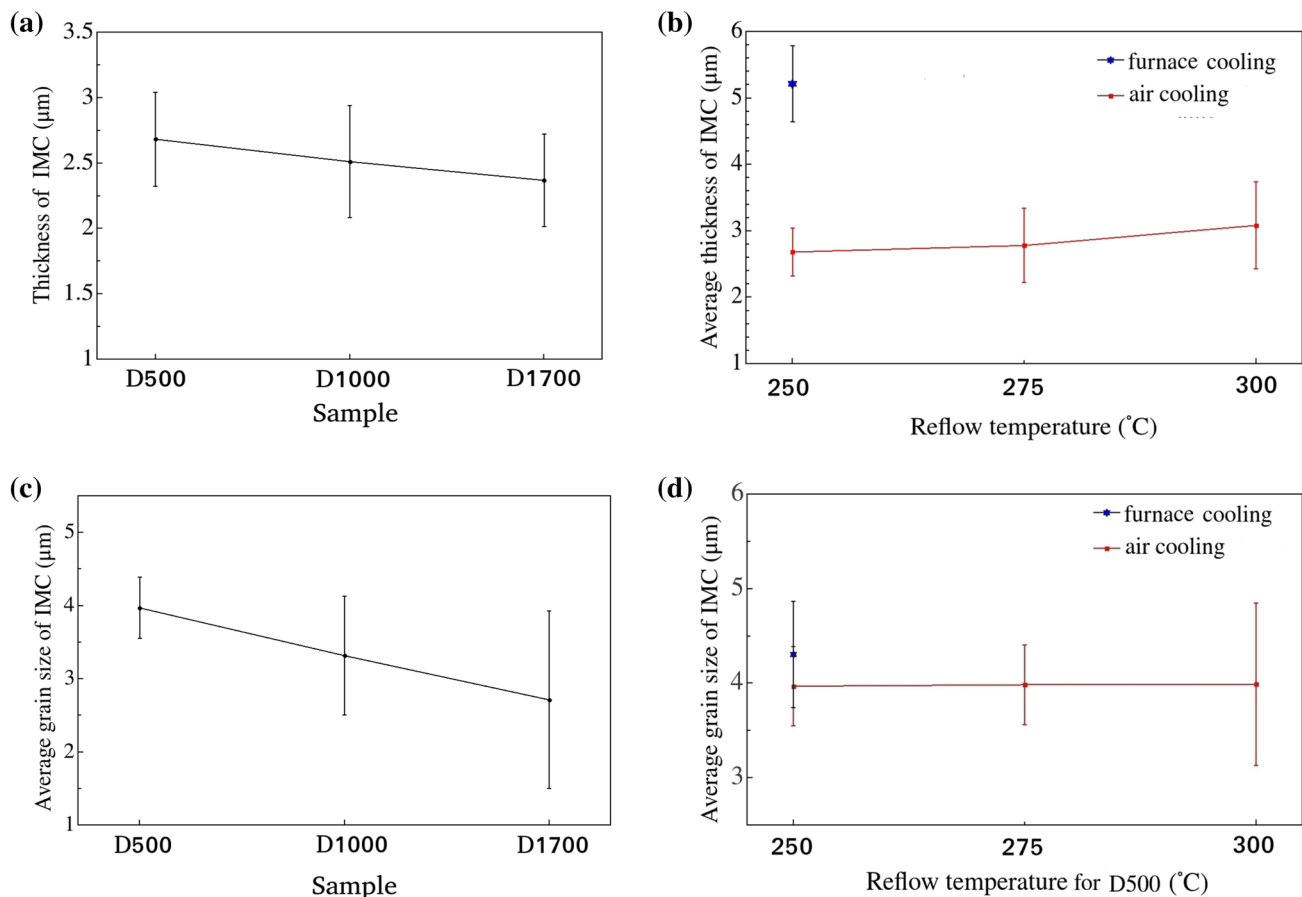
Fig. 19 Figures illustrating the effects of solder volume, temperature and cooling rate on peripheral IMC dimensions. For samples of different initial volume reflow soldered at 250 °C and subjected to air cooling, **a** average thickness and **c** grain size of IMC are presented graphically. In context of D500 sample subjected to isothermal reflow at several values of temperatures and processed for air cooling, the corresponding graphical plots of IMC thickness and grain diameters are presented in (**b**) and (**d**). The dimensions for furnace cooling experiment in D500 sample, as presented in (**b**) and (**d**), is only provided for the reflow at 250 °C

reflow at 250 °C, when the CR is increased by a factor of 100, the decrease in IMC thickness is 48.62 % and the decrease in grain size is 7.9 %. The increase in the IMC grain size and thickness, in case of slower cooling procedure (characterized with larger t) like furnace cooling owes to the larger volume ($V_{imc,prcpt}$) of precipitation driven IMC deposition on preexisting Cu_6Sn_5 surface, in accordance to the following expression [56]:

$$V_{imc,prcpt} = \frac{\pi V_o N \alpha^3 t^4}{3} \tag{7}$$

where, $V°$, N, α and t are respectively, original volume, rate of formation of IMC, number of precipitates per unit volume, and time.

For the D500 sample, with air cooling from varied initial reflow, it is revealed from Fig. 19b that the Cu_6Sn_5 IMC thickness corresponding to isothermal holding temperatures of 250, 275 and 300 °C are 2.68, 2.77 and 3.08 μm respectively respectively. The increment in IMC thickness of sample corresponding to 300 °C, as compared to that at 250 °C, is 14.9 %. As shown in Fig. 19d, the increase of grain diameter with the increment in reflow temperature from 250 to 300 °C is 0.5 %. However, the error bars in the figure show that the sample corresponding to larger temperatures have larger deviation from the mean value, thus indicating that greater reflow temperature results in the formation of IMCs widely varying from extremely larger to extremely smaller grain diameters.

In summary, at the peripheral interface of the solder joint consisting of extremely thin solder volume, the influencing factors for IMC thickness are in the order: cooling rate >> Reflow Temperature ≈ Solder Volume. In context of Cu_6Sn_5 IMC growing at the peripheral interface, solder

volume and cooling rate have a significant influence on the change of grain diameters, with the former having the greatest effect. The reflow temperature increase during air cooling experiments leads to the formation of IMCs with non-uniform grain diameters.

3.5 Interfacial reaction and growth mechanism of preferentially scalloped Cu_6Sn_5 at the peripheral regime

With the presentation of experimental data and analysis about IMC morphology characterization and size measurements, it is noteworthy how to describe the mathematical theory governing the growth mechanism of preferentially scalloped Cu_6Sn_5 at the peripheral interface of Sn/Cu joint. During reflow at constant temperature, flux driven ripening mechanism is the main characteristic phenomena for the growth of scalloped IMC. At the same time, as the cooling started, precipitation mechanism introduces flux driven grain growth of faceted IMC over the preexisting scalloped IMCs [19, 54, 55, 57–59].

For isothermal stage, growth of Cu_6Sn_5 intermetallic layer in Sn/Cu solid–liquid interface is a complex process. The inter-diffusion of species Cu and Sn, between liquid, interfacial Cu_6Sn_5 and solid Cu phases, has to be taken into account, if a detail mathematical model of IMC evolution has to be presented. However, for liquid solder/solid Cu substrate interface with IMC formation, the diffusion of Cu species from grain boundary channels between IMC bases,
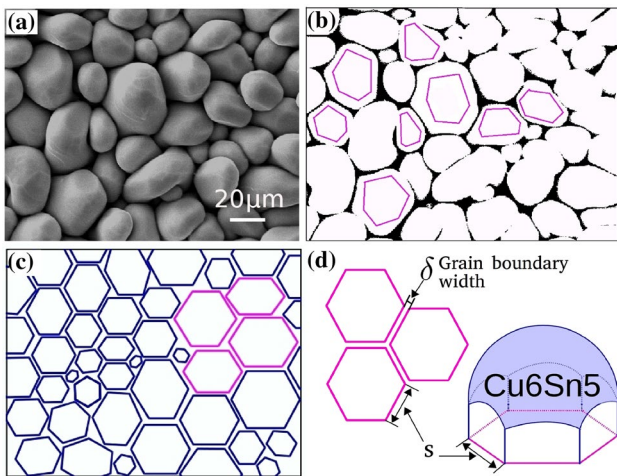

Fig. 20 Illustration of IMC morphology and grain boundaries of Cu_6Sn_5 compounds. The top-view morphology of peripheral IMC for D500 samples (250 °C, air cooling) are shown in (**a**). Image processing of (**a**) can exhibit the grain boundaries as in (**b**). The images of (**c**) and (**d**) are used to explain that Cu_6Sn_5 grains can be considered as grains having hexagonal base with spherical caps. The side length of hexagonal base is "s" and grain boundary channel between the grains is of width "δ"
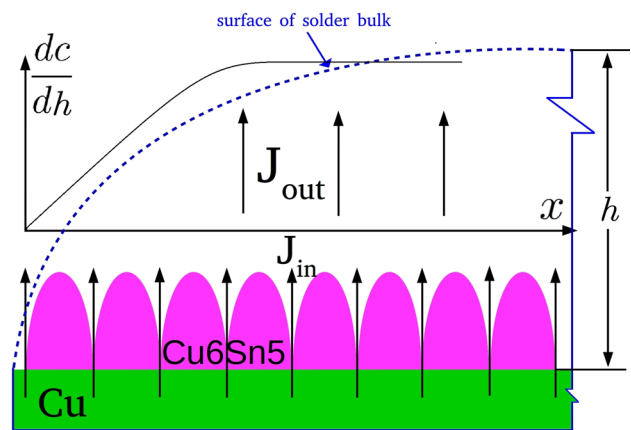

Fig. 21 A schematic sketch to explain the interference of solder height to Cu diffusion flux

can be sufficient to develop a simplified mathematical model for description of the kinetics of the interfacial reaction in Sn/Cu solder joints as well as the dissolution of Cu substrate [57, 58]. This research is focused on the mechanism of interfacial reaction for IMCs corresponding to thin solder film, and the mathematical model of IMC evolution remains the topic of future study.

Figure 20a is the top-view image of the scalloped morphology Cu_6Sn_5 at Sn/Cu interface of D500 sample soldering at 250 °C for 120 s under air cooling. After the processing of the image, the grain boundary of Cu_6Sn_5 can be clearly seen in Fig. 20b. As shown in Fig. 20b, c and d, scalloped Cu_6Sn_5 grains are assumed to have hexagonal base and spherical cap. In Fig. 20d, s is side length value of hexagon and $\delta \approx 2.5$ nm is the constant grain boundary channel width.

In order to understand the interfacial reaction kinetics in Fig. 21, the terms J_{in} and J_{out} are respectively defined as the influx of Cu from substrate to the Cu_6Sn_5/solder interfacial zone, and out-flux from interface to solder bulk. J_{in} is the sum of fluxes-grain boundary flux (J_{gb}) and flux via IMC grain volume (J_v). It can be consider as that consumption of the Cu substrate and subsequent interfacial reaction is grain boundary diffusion (channel diffusion) controlled during reflow-soldering process, it is considered that $J_{in} \approx J_{gb}$. Namely, the Cu atoms supplied by J_{in} feed the growth of interfacial Cu_6Sn_5 via Ostwald ripening. Consequently, a mathematical model on the kinetics of the interfacial reaction can be established based on the mass fluxes of J_{in} and J_{out}.

The mass influx of Cu atoms is mathematically expressed as:

$$J_{in} = D\phi_{GB}\frac{C_b - C_t}{s} \tag{8}$$

where D means the diffusivity of Cu atoms at grain boundary (liquid channel between neighboring grains, and it is

assumed equal to the diffusivity of Cu atoms in the liquid solder), C_t denotes the equilibrium concentration of Cu (in wt%) in solder at the planar interface between Cu_6Sn_5 and molten solder, and C_b is the equilibrium concentration of Cu (in wt%) in solder at the interface between substrate and solder at the bottom of grain boundary. ϕ_{GB} is the ratio of grain boundary (channel) area to the whole area. It can be described mathematically as:

$$\phi_{GB} = \frac{A_{gb}}{A_g + A_{gb}} = \frac{1}{\frac{\sqrt{3}}{2}s/\delta + 1} \tag{9}$$

where A_g and A_{gb} represents the interfacial areas occupied by IMC grains and grain boundaries, respectively, the total area A is expressed as $A_g + A_{gb}$.

Meanwhile, from Fick's first law, the mass out flux of Cu atoms can be expressed as:

$$J_{out} = -D\frac{dC}{dh} \tag{10}$$

where $\frac{dC}{dh}$ represents the Cu concentration gradient at the solder/Cu_6Sn_5 interface in the direction vertically from Cu substrate to the solder surface, as shown in Fig. 21.

Therefore, the net Cu flux from Cu substrate to the liquid solder bulk can be expressed as:

$$J_{net} = J_{in} - J_{out} = D\phi_{GB}\frac{C_{int} - C_{Sn}}{s} + D\frac{dC}{dh} \tag{11}$$

For thin films having smaller h and with a tendency to get supersaturated with Cu easily, we can assume that when t $\gg 0$ s, $\frac{dC}{dh} \approx 0$. The second term of RHS (right hand side) of Eq. 11 vanishes. So the first term contributes totally for ripening kinetics for enhanced scalloped IMC growth.

At the peripheral regime, the thickness of Cu_6Sn_5 or η layer during isothermal reflow soldering at a temperature T, $H_{\eta,isoT}$, can be expressed by the following formula [60]:

$$H_{\eta,isoT} = H_{\eta,total} - \frac{C_s\rho_{Sn}M_\eta h_{Sn}}{(6 - 11C_s)\rho_\eta M_{Sn}} \tag{12}$$

where, $H_{\eta,total}$ is the measured average thickness of the Cu_6Sn_5 layers at the Sn/Cu interface after soldering, and ρ and M with subscripts representing Sn and η are the corresponding densities and molar weights of solder and IMC phase, respectively. Moreover, C_s is the saturated at.% of Cu in the molten Sn at the isothermal hold temperature of 250 °C. The last term in Eq. 12 accounts for the thickness of Cu_6Sn_5 due to the precipitation out of excessive Cu in the liquid Sn during cooling. The thickness of η phase is directly proportional to the solder height.

Equation 12 is derived from experimental measurements in the work of Ref. [60] and it can be utilized to deduce

theoretical expressions on the IMC thickness yielded by J_{in} of Eq. 11 at constant temperature temperature reflow. An increase in solder height h or h_{Sn} is supposed to increase the cooling based IMC thickness. On the other hand, solders with smallest height at periphery (D500) have the largest IMC thickness, overshadowing the effect of cooling only. This must imply that the lowered thickness of solder film must cause an increase in Ostwald ripening based IMC thickening several times greater than the counter effect during cooling. The following expression can empirically relate isothermal reflow based Cu_6Sn_5 layers thickness (H_{IMC}) to solder film height (h).

$$H_{IMC} = a(1 - b \times h)^n \tag{13}$$

where, a and b are empirical constants and the exponent n > 1.

4 Conclusions

The following conclusions can be made from this study:

1. The effects of solder volume, reflow temperature and cooling rate on the growth behavior of preferentially scalloped Cu_6Sn_5 IMCs at the peripheral Sn/Cu interface have been assessed.

2. For solder balls of initial diameters of 500, 1000 and 1700 µm (sample ID: D500, D1000 and D1700), reflowed at 250 °C and subjected to air cooling, the thickness of peripheral strip consisting of dominantly scalloped intermetallic compounds, increased with an increase in solder volume. After spreading, the maximum height of the solder at the inward peripheral regime, wherein IMC retain the scallop morphology was the greatest for D1700 sample and smallest for D500 samples. The finite element analysis of Cu diffusion at the peripheral solder volume, has shown that D500 samples gets saturated the earliest and D1700 the latest. This size effect provides the basis for existence of enhanced IMC layer thickness and grain diameter in smaller solder samples.

3. In context of D500 sample, for air cooling from reflow temperature of 250 °C, scalloped IMCs with almost no facets are present in the peripheral regime. As the reflow temperature increased, faceted planes appear on the Cu_6Sn_5 surface. The IMC layer thickness increases with an increase in reflow temperature. The raise in the magnitude of reflow temperature is also associated with the non-uniformity of grain diameters of the intermetallic compounds.

4. Compared to the air cooling experiment, the D500 sample furnace cooled from reflow temperature of 250 °C resulted in peripheral IMC with significantly

larger layer thickness and grain diameter. In contrary to the IMCs of D500 (300 °C, air cooled) characterized by a few large facets over the scalloped morphology; the IMCs for this furnace cooled sample consisted of many many tiny facets over the scallop shape.

5. The lowering of solder height at the periphery can enhance the rate of Ostwald ripening mechanism and enforce the shortage of Cu supply during cooling procedure.

References

1. W. Zhou, H. Zhang, W. Ping, Whisker growth in Sn and SnPb thin films under electromigration. Vacuum **107**, 103–107 (2014)
2. W.H. Kohl, Soldering and brazing. Vacuum **14**, 175–198 (1964)
3. A. Kunwar, H. Ma, J. Sun, S. Li, J. Liu, Modeling the diffusion-driven growth of a pre-existing gas bubble in molten tin. Met. Mater. Int. **21**(5), 962–970 (2015)
4. A. Kunwar, H. Ma, H. Ma, J. Sun, N. Zhao, M. Huang, On the increase of intermetallic compound's thickness at the cold side in liquid Sn and SnAg solders under thermal gradient. Mater. Lett. **172**(August), 211–215 (2016)
5. H. Ma, A. Kunwar, J. Sun, B. Guo, H. Ma, In situ study on the increase of intermetallic compound thickness at anode of molten tin due to electromigration of copper. Scr. Mater. **107**, 88–91 (2015)
6. Y. Tang, S. Luo, G. Li, Z. Yang, C. Hou, Ripening growth kinetics of Cu_6Sn_5 grains in Sn-3.0Ag-0.5Cu-xTiO$_2$/Cu solder joints during the reflow process. J. Electron. Packag. **140**(1), 011003 (2018)
7. X. Zhang, H. Xiaowu, X. Jiang, Y. Li, Effect of Ni addition to the Cu substrate on the interfacial reaction and IMC growth with $Sn_{3.0}Ag_{0.5}Cu$ solder. Appl. Phys. A **124**(4), 1–13 (2018)
8. B. Liu, Y. Tian, J. Feng, C. Wang, Enhanced shear strength of CuSn intermetallic interconnects with interlocking dendrites under fluxless electric current-assisted bonding process. J. Mater. Sci. **52**(4), 1943–1954 (2017)
9. S. Annuar, R. Mahmoodian, M. Hamdi, K.N. Tu, Intermetallic compounds in 3D integrated circuits technology: a brief review. Sci. Technol. Adv. Mater. **18**(1), 1–11 (2017)
10. K.N. Tu, Y. Liu, M. Li, Effect of Joule heating and current crowding on electromigration in mobile technology. Appl. Phys. Rev. **4**(1), 011101 (2017)
11. M.L. Huang, F. Yang, Size effect model on kinetics of interfacial reaction between Sn-xAg-yCu solders and Cu substrate. Sci. Rep. **4**(November), 7117 (2014)
12. J. Feng, C. Hang, Y. Tian, B. Liu, C. Wang, Growth kinetics of Cu_6Sn_5 intermetallic compound in Cu-liquid Sn interfacial reaction enhanced by electric current. Sci. Rep. (2018). https://doi.org/10.1038/s41598-018-20100-1
13. J.Q. Huang, M.B. Zhou, S.B. Liang, X.P. Zhang, Size effects on the interfacial reaction and microstructural evolution of Sn-ball/

14. F. Sun, Y. Zhu, X. Li, Effects of micro solder joint geometry on interfacial IMC growth rate. J. Electron. Mater. **46**(7), 4034–4038 (2017)
15. S. Wang, Y. Yao, X. Long, Size effect on microstructure and tensile properties of $Sn_{3.0}Ag_{0.5}Cu$ solder joints. J. Mater. Sci. Mater. Electron. **28**(23), 17682–17692 (2017)
16. H. Ma, R.A. Kunwar, J.C. Huang, Y. Wang, N. Zhao, H. Ma, Size effect on IMC growth induced by Cu concentration gradient and pinning of Ag_3Sn particles during multiple reflows. Intermetallics **90**(May), 90–96 (2017)
17. C.C. Chang, Y.W. Lin, Y.W. Wang, C.R. Kao, The effects of solder volume and Cu concentration on the consumption rate of Cu pad during reflow soldering. J. Alloys Compd. **492**(1–2), 99–104 (2010)
18. T.L. Yang, J.J. Yu, W.L. Shih, C.H. Hsueh, C.R. Kao, Effects of silver addition on CuSn microjoints for chip-stacking applications. J. Alloys Compd. **605**, 193–198 (2014)
19. A. Kunwar, B. Guo, S. Shang, P. Råback, Y. Wang, J. Chen, H. Ma, X. Song, N. Zhao, Roles of interfacial heat transfer and relative solder height on segregated growth behavior of intermetallic compounds in Sn/Cu joints during furnace cooling. Intermetallics **93**, 186–196 (2018)
20. B. Guo, H. Ma, C. Jiang, Y. Wang, A. Kunwar, N. Zhao, M. Huang, Formation mechanism and kinetic analysis of the morphology of Cu_6Sn_5 in the spherical solder joints at the Sn/Cu liquid-solid interface during soldering cooling stage. J. Mater. Sci. Mater. Electron. **28**(7), 5398–5406 (2017)
21. H. Xie, B. Deng, G. Du, Y. Fu, Y. He, H. Guo, G. Peng, Y. Xue, G. Zhou, Y. Ren, Y. Wang, R. Chen, Y. Tong, T. Xiao, X-ray biomedical imaging beamline at SSRF. J. Instrum. **8**(8), C08003 (2013)
22. B. Guo, A. Kunwar, C. Jiang, N. Zhao, J. Sun, J. Chen, Y. Wang, M. Huang, H. Ma, Synchrotron radiation imaging study on the rapid IMC growth of SnxAg solders with Cu and Ni substrates during the heat preservation stage. J. Mater. Sci. Mater. Electron. **29**(1), 589–601 (2018)
23. H. Ma, Y. Wang, J. Chen, A. Kunwar, H. Ma, N. Zhao, Geometrical outline evolution and size-inhibiting interaction of interfacial solder bubbles and IMCs during multiple reflows. Vacuum **145**, 103–111 (2017)
24. N. Eustathopoulos, Wetting by liquid metals application in materials processing: the contribution of the grenoble group. Metals **5**(1), 350–370 (2015)
25. W. Villanueva, W.J. Boettinger, G.B. McFadden, J.A. Warren, A diffuse-interface model of reactive wetting with intermetallic formation. Acta Mater. **60**(9), 3799–3814 (2012)
26. F. Wang, A. Reiter, M. Kellner, J. Brillo, M. Selzer, B. Nestler, Phase-field modeling of reactive wetting and growth of the intermetallic Al_2Au phase in the Al-Au system. Acta Mater. **146**, 106–118 (2018)
27. A. Yakymovych, V. Sklyarchuk, Y. Plevachuk, B. Sokoliuk, Viscosity and electrical conductivity of the liquid Sn-3.8Ag-0.7Cu alloy with minor co admixtures. J. Mater. Eng. Perform. **25**(10), 4437–4443 (2016)
28. J. Hektor, M. Ristinmaa, H. Hallberg, S.A. Hall, S. Iyengar, Coupled diffusion-deformation multiphase field model for elastoplastic materials applied to the growth of Cu_6Sn_5. Acta Mater. **108**, 98–109 (2016)
29. M.S. Park, S.L. Gibbons, R. Arróyave, Phase-field simulations of intermetallic compound evolution in Cu/Sn solder joints under electromigration. Acta Mater. **61**(19), 7142–7154 (2013)

30. B.S. Kirk, J.W. Peterson, R.H. Stogner, G.F. Carey, libMesh: a C++ library for parallel adaptive mesh refinement/coarsening simulations. Eng. Comput. **22**(3–4), 237–254 (2006)

31. D. Gaston, C. Newman, G. Hansen, D. Lebrun-Grandié, MOOSE: a parallel computational framework for coupled systems of nonlinear equations. Nucl. Eng. Des. **239**(10), 1768–1778 (2009)

32. M.R. Tonks, D. Gaston, P.C. Millett, D. Andrs, P. Talbot, An object-oriented finite element framework for multiphysics phase field simulations. Comput. Mater. Sci. **51**(1), 20–29 (2012)

33. D. Schwen, L.K. Aagesen, J.W. Peterson, M.R. Tonks, Rapid multiphase-field model development using a modular free energy based approach with automatic differentiation in MOOSE/MARMOT. Comput. Mater. Sci. **132**, 36–45 (2017)

34. S. Shang, A. Kunwar, J. Yao, Y. Wang, N. Zhao, M. Huang, H. Ma, All-round suppression of Cu_6Sn_5 growth in Sn/Cu joints by utilizing TiO_2 nanoparticles. J. Mater. Sci. Mater. Electron. **29**(18), 15966–15972 (2018)

35. P.G. Kim, J.W. Jang, T.Y. Lee, K.N. Tu, Interfacial reaction and wetting behavior in eutectic SnPb solder on Ni/Ti thin films and Ni foils. J. Appl. Phys. **86**(12), 6746–6751 (1999)

36. R.G. Cox, The dynamics of the spreading of liquids on a solid-surface. Part 1. viscous-flow. J. Fluid Mech. **168**, 169–194 (1986)

37. A. Ribes, C. Caremoli, Salome platform component model for numerical simulation. In *31st Annual International Computer Software and Applications Conference, vol 2—(COMPSAC 2007)*, pp. 553–564

38. C.H. Ma, R.A. Swalin, A study of solute diffusion in liquid tin. Acta Metall. **8**(6), 388–395 (1960)

39. M.L. Huang, T. Loeher, A. Ostmann, H. Reichl, Role of Cu in dissolution kinetics of Cu metallization in molten Sn-based solders. Appl. Phys. Lett. **86**(18), 1–3 (2005)

40. M.J. Rizvi, H. Lu, C. Bailey, Modeling the diffusion of solid copper into liquid solder alloys. Thin Solid Films **517**(5), 1686–1689 (2009)

41. O.M. Abdelhadi, L. Ladani, IMC growth of Sn-3.5Ag/Cu system: combined chemical reaction and diffusion mechanisms. J. Alloys Compd. **537**, 87–99 (2012)

42. M. Malinen, P. Raback, Elmer finite element solver for multiphysics and multiscale problems. Multiscale Model. Methods Appl. Mater. Sci. **19**, 101–113 (2013)

43. U. Ayachit, A. Bauer, A. Chaudhary, D. DeMarle, B. Geveci, S. Jourdain, K. Lutz, P. Marion, R. Maynard, N. Shetty, Y. Yuan, *The ParaView Guide* (Kitware Inc., Clifton Park, 2008)

44. O.Y. Liashenko, F. Hodaj, Wetting and spreading kinetics of liquid Sn on Ag and Ag_3Sn substrates. Scr. Mater. **127**, 24–28 (2017)

45. N. Eustathopoulos, Progress in understanding and modeling reactive wetting of metals on ceramics. Curr. Opin. Solid State Mater. Sci. **9**(4–5), 152–160 (2005)

46. D.G.A.L. Aarts, H.N.W. Lekkerkerker, H. Guo, G.H. Wegdam, D. Bonn, Hydrodynamics of droplet coalescence. Phys. Rev. Lett. **95**, 1–4 (2005)

47. W. Villanueva, W.J. Boettinger, J.A. Warren, G. Amberg, Effect of phase change and solute diffusion on spreading on a dissolving substrate. Acta Mater. **57**(20), 6022–6036 (2009)

48. F. Wang, B. Nestler, A phase-field study on the formation of the intermetallic Al_2Au phase in the Al-Au system. Acta Mater. **95**, 65–73 (2015)

49. E. Saiz, R.M. Cannon, A.P. Tomsia, Reactive spreading: adsorption, ridging and compound formation. Acta Mater. **48**(18–19), 4449–4462 (2000)

50. R.L. Panton, J.W. Lee, L. Goenka, A. Achari, Simulation of void growth in molten solder bumps. J. Electron. Packag. **125**(3), 329 (2003)

51. J.W. Xian, S.A. Belyakov, M. Ollivier, K. Nogita, H. Yasuda, C.M. Gourlay, Cu_6Sn_5 crystal growth mechanisms during solidification of electronic interconnections. Acta Mater. **126**, 540–551 (2017)

52. D. Frear, D. Grivas, J.W. Morris, The effect of Cu_6Sn_5 whisker precipitates in bulk 60Sn-40Pb solder. J. Electron. Mater. **16**(3), 181–186 (1987)

53. F. Meng, S.A. Morin, A. Forticaux, S. Jin, Screw dislocation driven growth of nanomaterials. ACC Chem. Res. **46**(7), 1616–1626 (2013)

54. M. Schaefer, R.A. Fournelle, J.I.N. Liang, Theory for intermetallic phase growth between Cu and liquid Sn-Pb solder based on grain boundary diffusion control. Electron. Mater. **27i**, 1167–1176 (1998)

55. K.N. Tu, A.M. Gusak, M. Li, Physics and materials challenges for lead-free solders. J. Appl. Phys. **93**(3), 1335–1353 (2003)

56. H. Ma, A. Kunwar, B. Guo, J. Sun, C. Jiang, Y. Wang, X. Song, N. Zhao, H. Ma, Effect of cooling condition and Ag on the growth of intermetallic compounds in Sn-based solder joints. Appl. Phys. A Mater. Sci. Process. **122**(12), 1–10 (2016)

57. H.K. Kim, K.N. Tu, Kinetic analysis of the soldering reaction between eutectic SnPb alloy and Cu accompanied by ripening. Phys. Rev. B **53**(23), 16027–16034 (1996)

58. A.M. Gusak, K.N. Tu, Kinetic theory of flux-driven ripening. Phys. Rev. B. Condens. Matter Mater. Phys. **66**(11), 1–14 (2002)

59. J. Kukelhan, *Copper Tin Intermetallic Crystals and Their Role in the Formation of Microbridges between the Leads of Hand Reworked Fine Pitch Components* (IPC-assocation Connect. Eletron. Ind., Lasvegas, 2010)

60. J.F. Li, P.A. Agyakwa, C.M. Johnson, Interfacial reaction in Cu/Sn/Cu system during the transient liquid phase soldering process. Acta Mater. **59**(3), 1198–1211 (2011)